Magnetization Reversals of $Fe_{81}Ga_{19}$-Based Flexible Thin Films Under Multiaxial Mechanical Stress

F. Legall,[1] C. Morice,[1] W. Jahjah,[1] A. Bivic,[1] N. Ryon,[1] J. Richy,[1] A.R.E. Prinsloo,[2] C.J. Sheppard,[2] A. Fessant,[1] J.-Ph. Jay,[1] D. Spenato,[1] and D.T. Dekadjevi[1,2,*]

[1] *Laboratoire d'Optique et de Magnétisme (OPTIMAG), EA 938, IBSAM, Université de Bretagne Occidentale, Brest 29200, France*

[2] *Cr Research Group, Department of Physics, University of Johannesburg, PO Box 524, Auckland Park 2006, South Africa*

(Received 8 July 2020; revised 22 February 2021; accepted 11 March 2021; published 19 April 2021)

The effect of multiaxial mechanical stress on angle-dependent magnetization reversals is studied on a single 10-nm $Ni_{80}Fe_{20}$ film, a single 10-nm $Fe_{81}Ga_{19}$ film, and a $Ni_{80}Fe_{20}$(10 nm)/$Fe_{81}Ga_{19}$(10 nm) bilayer. These films are grown on flexible Al "kitchenlike" foils. These flexible foils are bent on two convex optical lenses to apply multiaxial mechanical stresses of different magnitudes. In order to understand the mechanisms driving the physical properties of the flexible systems, the magnetic films are also grown on hard native-oxide-covered Si(100) substrates. By probing the angular dependence of the coercive field and the remanent magnetization, we show that the $Ni_{80}Fe_{20}$ single layer and the $Ni_{80}Fe_{20}/Fe_{81}Ga_{19}$ bilayer grown on Si present a uniaxial anisotropy. Along their easy axis, their domain structure at the coercive field exhibits large domains with sawtooth domain walls. However, the $Fe_{81}Ga_{19}$ layer grown on Si shows a cubic anisotropy and sharp domain walls with a right-angle geometry along its easy axis. All layers grown on Al foils show development or enhancement of a uniaxial anisotropy arising from the Al surface morphology. Multiaxial mechanical stress applied to the flexible Al foils results in very different nonreversible effects as a function of the composition of the layered system. For $Ni_{80}Fe_{20}$, multiaxial mechanical stress has no effect, as expected for a nonmagnetostrictive system. For $Fe_{81}Ga_{19}$, it results in a full in-plane randomization of its magnetization-reversal properties. For the bilayer, multiaxial mechanical stress does not fully randomize the in-plane magnetization-reversal properties: the bilayer retains a uniaxial character.

DOI: 10.1103/PhysRevApplied.15.044028

I. INTRODUCTION

Magnetostrictive thin films have attracted a great deal of interest in the last few decades. Firstly, this is because of a need to understand the fundamental mechanisms driving the strain and magnetic coupling in thin films. Secondly, this interest originates from the fact that magnetostrictive properties are of use in sensing devices, actuators, energy harvesters, and spintronic devices [1,2]. Among the different magnetostrictive alloys, $Fe_{81}Ga_{19}$, discovered in 2000 by Clark *et al.* [3], has received particular attention as it exhibits remarkable properties such as low hysteresis, large magnetostriction, good tensile strength, and machinability, and there has been recent progress in commercially viable methods of processing [4]. The main advantage of $Fe_{81}Ga_{19}$ alloys when compared with the rare-earth-alloy family is reduced cost, as well as the fact that these alloys are less brittle.

Magnetostrictive thin films, including those prepared using $Fe_{81}Ga_{19}$ alloys, can be used for making electronic circuits and devices on flexible substrates [5–7]. Their magnetic properties are inherently sensitive to mechanical deformation through the inverse magnetostrictive effect (also referred to as the Villari effect). A magnetostrictive material may exhibit reversible magnetic properties that change when it is subjected to elastic strain, whereas a magnetostrictive material subjected to a plastic residual strain may exhibit irreversible changes in its magnetic properties. The interest in flexible devices has its origin in the fact that these devices are significantly lower in cost, as well as lighter and more compact, compared with conventional devices. Also, various flexible devices, displays, logic devices, sensors, and memories are expected to be integrated into multifunctional systems, and to be implemented in wearable technologies [8,9]. Consequently, flexible magnetostrictive systems constitute an essential part of the field named straintronics [10]. In particular, the attributes of $Fe_{81}Ga_{19}$ introduce opportunities for the use of a smart material in applications that involve stretching, bending, shear, or torsion.

Among the different properties of magnetostrictive flexible thin films to be understood, their magnetization

*david.dekadjevi@univ-brest.fr

reversals (MRevs), which are related to the magnetic-moment direction under external stimuli, including electrical, magnetic, or mechanic stimuli, are of interest for applications and fundamental studies [6]. MRevs are driven by the anisotropic properties, which determine the application areas of the thin film and the associated performance of devices. For instance, the magnetic sensitivity of sensors is related to magnetization reversals and magnetic-anisotropy properties. Consequently, tailoring and understanding MRevs of flexible $Fe_{81}Ga_{19}$ thin films would be of prime interest for actuators, transducers, and energy-harvesting devices.

Following this scientific goal, the MRev behavior of $Fe_{81}Ga_{19}$ thin films grown on flexible substrates has attracted a great deal of attention in the last decade [11–17]. These previous studies focused on the MRev properties of flexible $Fe_{81}Ga_{19}$ under tensile or compressive uniaxial mechanical stress (UMS). The main idea was to achieve different MRev properties in order to identify the potential of flexible $Fe_{81}Ga_{19}$ for applications. In addition, these studies revealed large modifications of the MRev properties due to UMS [11,13–15,17–19]. It should be noted that UMS resulted in differences in MRev properties that were found to be irreversible, in the sense that the virgin state before UMS could not be recovered once UMS was applied. This irreversibility property allows stabilization of the MRevs of flexible $Fe_{81}Ga_{19}$ and may enlarge the potential applications of this system.

Whereas the use of UMS with flexible $Fe_{81}Ga_{19}$ thin films has previously been considered in order to tailor stable MRev properties of $Fe_{81}Ga_{19}$, multiaxial mechanical stress (MMS) has not been not studied, despite its key role in applications [20–25]. MMS needs to be considered, as many different combinations and orientations of magnetic fields and mechanical stresses can occur in real devices and applications. Wearable electronics may be subjected to a wide range of directional distributed external stresses. Stretchable sensors capable of detecting different mechanical stimuli are essential in wearable applications involving multiaxial motion [26]. MMS is of interest in the field of soft robotics and smart prosthetics for applications in artificial intelligent skin [27–29]. In order to understand external environments or stimuli in an accurate manner, electronic skin needs to perceive various types of mechanical information (i.e., multiaxial information) so that it can emulate human perception and natural touch. In addition, MMS is purposely used for converting mechanical energy into electrical energy for energy-harvesting purposes [21–23]. Finally, MMS needs to be taken into consideration in transformers, as it may be detrimental when it occurs in electromagnetic devices, where magnetostrictive properties play a key role in generating detrimental noise [24]. Despite all this, the effects of MMS on the MRev properties of $Fe_{81}Ga_{19}$ thin films have been overlooked and not yet studied.

In this paper, we report on the effect of MMS on magnetization reversals in flexible $Fe_{81}Ga_{19}$-based thin films. This effect is studied on a single 10-nm $Ni_{80}Fe_{20}$ (Py) film, on a single 10-nm $Fe_{81}Ga_{19}$ film, and on a Py(10 nm)/$Fe_{81}Ga_{19}$(10 nm) bilayer. These films are grown on flexible Al "kitchenlike" foils. MMS can take a variety of forms, from biaxial to isotropic. Before approaching an anisotropic MMS geometry such as a biaxial one, the isotropic case is of interest for probing the effect of a fully randomized MMS on MRevs. Consequently, Al foils are bent on two convex optical lenses of different curvature radius to achieve a tensile stress that is isotropic in the film plane with two different magnitudes.

The Al foil substrate is chosen as it is flexible, inexpensive, durable, and greaseproof, and the raw materials required for its manufacture are plentiful. Also, the morphology of Al foils presents a grooved surface due to the rolling process used in its industrial production [30]. This surface may lead to MRev properties of interest with or without MMS. In general, in comparing the properties of flexible films with those of inflexible ones, is of interest to achieve an understanding of the mechanisms driving the physical properties of flexible films. For this reason, in this investigation all magnetic films are also grown on hard native-oxide-covered Si(100) substrates, as these substrates are an archetype of flat and hard substrates.

$Fe_{81}Ga_{19}$ is chosen for its magnetostrictive properties of interest. The $Ni_{80}Fe_{20}$ film is permalloy. It is chosen as it constitutes an archetype of a soft magnetic material, and as it is considered as a nonmagnetostrictive reference. Beyond the single-film case, a study of a bilayer made of Py and $Fe_{81}Ga_{19}$ is performed to probe possible hybridization of the MRev properties, with and without MMS, at the nanoscale. Indeed, interfacing different magnetic thin films is a mechanism for tailoring magnetic properties in general. This mechanism has been shown to be of interest for driving magnetic properties of nonflexible magnetostrictive bilayers [31–35], including nonflexible Py/$Fe_{81}Ga_{19}$ bilayers [33–35]. However, there has been no previous work studying magnetic properties of flexible Py/$Fe_{81}Ga_{19}$ bilayers.

In the first part of this paper, the experimental details and procedures are introduced. In the second part, the MRev properties of films on hard Si substrates are presented. In the third part, the MRev properties of films on flexible Al foils and their dependence on MMS are presented. In the last part of this paper, conclusions are drawn.

II. EXPERIMENTAL DETAILS

In the study presented in this paper, a 10-nm $Fe_{81}Ga_{19}$ thin film, a 10-nm Py thin film, and an $Fe_{81}Ga_{19}$(10 nm)/Py(10 nm) bilayer are grown on Si substrates and Al foils by a sputtering technique. All samples are covered with a 5-nm-thick Ta cap layer to avoid oxidation.

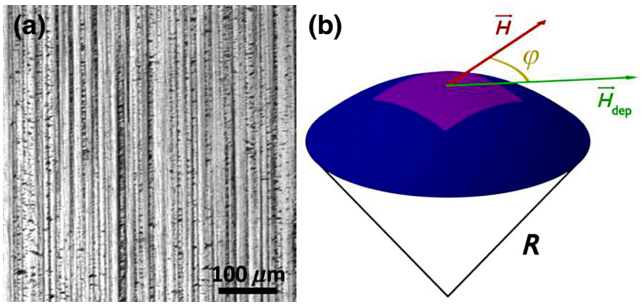

FIG. 1. (a) Scanning-electron-microscope image of the surface morphology of the Al foil. (b) Schematic illustration of an Al foil on top of a convex optical lens. $\varphi = 0$ when the applied field H during MOKE measurements is in the same direction as H_{dep}, the applied magnetic field during growth.

An $Fe_{81}Ga_{19}$ target and a $Ni_{80}Fe_{20}$ target are used. Sample compositions are confirmed by utilizing electron-probe microanalysis measurements. The base pressure prior to film deposition is typically 10^{-7} mbar. The rf power used to sputter the 3-in. $Fe_{81}Ga_{19}$ ($Ni_{80}Fe_{20}$) target is 100 (100) W, and the argon pressure is 1.5×10^{-2} (10^{-2}) mbar. With these sputtering conditions, the growth rate for the $Fe_{81}Ga_{19}$ ($Ni_{80}Fe_{20}$) films is 0.22 (0.20) nm/s. The growth is carried out under an in-plane magnetic field $H_{dep} \sim 2.4$ kA m^{-1} (300 Oe), in order to favor a preferential magnetic-anisotropy direction.

The thin films are grown on commercially available native-oxide-covered (100) Si substrates [36] and on flexible kitchen-type aluminum foils. The Si substrates are 500-μm-thick rigid substrates and exhibit a root-mean-square roughness below 0.5 nm. The Al foils are 20-μm-thick flexible substrates. Scanning-electron-microscope measurements reveal the typical grooved surface morphology of the Al foils [30], as shown in Fig. 1(a). This grooved surface arises from the rolling mechanism used to achieve the Al foils. The width of the grooves is found to be typically in the order of 10 μm. The Al foils exhibit a root-mean-square roughness of 0.53 μm and an arithmetic average roughness of 0.39 μm. It should be noted here that H_{dep} is systematically applied parallel to the grooves during the growth of the thin films.

Once the magnetic layers have been grown on flat Al foils, magnetization reversals are studied on flat and on spherically curved Al foils. To achieve the bending and the resulting MMS, Al foils are stuck onto convex optical lenses, as shown in Fig. 1(b). Two different lenses are used to allow MMSs of different magnitudes. The radius of curvature of the first convex optical lens is 24.0 cm, and that of the second is 58.0 cm. Because of the dome shape of the convex optical lenses, the bending stresses the substrate; the stress is tensile with axial symmetry, and the film deposited onto the external surface is stressed isotropically in the film plane [37,38]. It should be noted here that structural characterizations involving confocal microscopy, scanning electron microscopy, and transmission electron microscopy are performed on the samples before and after bending. These characterizations do not reveal the presence of extended defects (such as cracks) resulting from the bending procedure.

TABLE I. Samples on Si substrates studied in Sec. III. R is the radius of curvature, as seen in Fig. 1(b).

Sample name	R	Layer structure
Py^{Si}	∞	$Ni_{80}Fe_{20}$(10 nm)/Si
$FeGa^{Si}$	∞	$Fe_{81}Ga_{19}$(10 nm)/Si
$Bilayer^{Si}$	∞	$Fe_{81}Ga_{19}$(10 nm)/$Ni_{80}Fe_{20}$(10 nm)/Si

Magnetic properties at room temperature are determined using the magneto-optic Kerr effect (MOKE) in a wide-field Kerr microscope from Evico Magnetics [39,40].

III. MAGNETIZATION REVERSALS ON Si SUBSTRATES

In this section, MRevs of Py, $Fe_{81}Ga_{19}$, and Py/$Fe_{81}Ga_{19}$ layers grown on Si substrates are reported. The samples studied in this section and their characteristics are summarized in Table I. In the following, $\varphi = 0$ when the applied field during the MOKE measurements is in the same direction as H_{dep}, the applied magnetic field during growth.

A. Py on Si

Figure 2(a) presents the magnetization-reversal loops for Py^{Si}. The MRev loop along $\varphi = 0°$ exhibits a rectangular shape and a rather small coercive field (H_c) of 2.8 Oe. The loop along $\varphi = 90°$ exhibits very weak hysteresis, with an H_c of 1.0 Oe and a small normalized remanence (M_R/M_s) of 0.13. These MRev-loop properties along and perpendicular to the applied deposition field correspond to a soft magnetic system with a growth-induced uniaxial anisotropy, as expected for a Py thin film grown under an external field [41]. The nonvanishing H_c and M_R/M_s perpendicular to H_{dep} indicate the presence of an anisotropy dispersion.

The domain configuration along the easy axis (EA) is probed in the vicinity of the coercive field, as shown in Fig. 2(b). It exhibits a zigzag (also referred to as "sawtooth") domain-wall configuration, separating large domains. This particular configuration of domain walls is observed in magnetic thin films with in-plane uniaxial anisotropy [42], and has been previously reported for Py thin films [43,44]. Zigzag domains walls are formed between two areas with opposite head-on magnetization directions; they minimize the magnetostatic energy, thereby reducing the charge density but increasing the

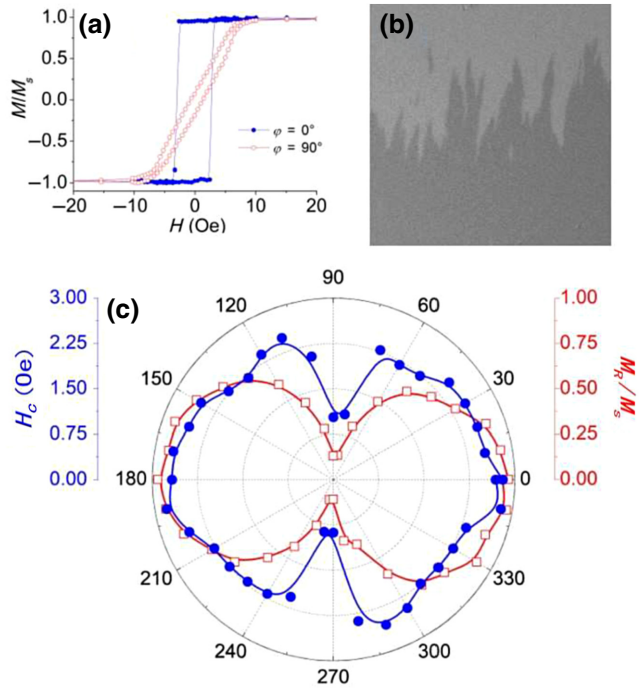

FIG. 2. For Py^{Si}, (a) hysteresis loops measured along $\varphi = 0°$ (filled black circles) and along $\varphi = 90°$ (open red circles); (b) 5 mm × 5 mm MOKE image obtained in the vicinity of the coercive field along $\varphi = 0°$; (c) angular dependence of H_c (filled blue circles) and M_R/M_s (red squares).

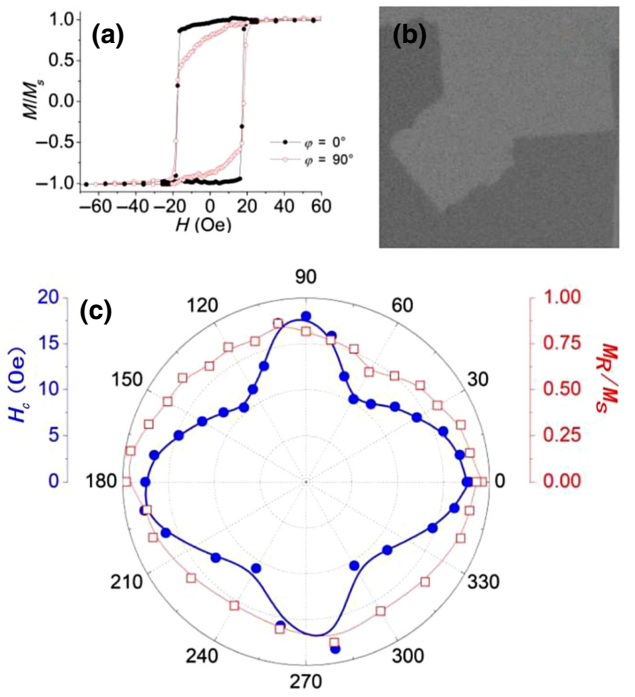

FIG. 3. For $FeGa^{Si}$, (a) hysteresis loops measured along $\varphi = 0°$ (filled black circles) and along $\varphi = 90°$ (open red circles); (b) 5 mm × 5 mm MOKE image obtained in the vicinity of the coercive field along $\varphi = 0°$; (c) angular dependence of H_c (filled blue circles) and M_R/M_s (red squares).

length of the wall, with the charge distributed on both sides of the wall [45].

Systematic in-plane angle-dependent measurements are performed on the Py sample to further probe the anisotropic character. For each applied magnetic field direction, the angular dependences of H_c and M_R/M_s are obtained, as shown in Fig. 2(c). Both angular dependences are typical of a uniaxial system, as the H_c polar plot exhibits a butterflylike shape and the M_R/M_s plot exhibits clear symmetrical lobes [46,47]. The angle-dependent study shows that the uniaxial EA is aligned with H_{dep}.

B. $Fe_{81}Ga_{19}$ on Si

For $FeGa^{Si}$, the MRev loop along $\varphi = 0°$ exhibits a rectangular shape with an H_c of 18 Oe, as shown in Fig. 3(a). The loop along $\varphi = 90°$ exhibits the same H_c as that along $\varphi = 0°$. This indicates that $FeGa^{Si}$ is not uniaxial. The domain configuration along $\varphi = 0°$ is probed in the vicinity of the coercive field, as shown in Fig. 3(b). The domain pattern in $FeGa^{Si}$ differs substantially from that in Py^{Si}. The domain size is still large, but the transition between two regions is quite sharp and does not exhibit a zigzag shape. A right-angle boundary between two domains is observed, which suggests the presence of a cubic anisotropy (i.e., a fourfold anisotropy).

Systematic in-plane angle-dependent measurements of H_c and M_R/M_s are performed on $FeGa^{Si}$ to probe further the anisotropic character, as shown in Fig. 3(c). The angular dependence of H_c exhibits four well-defined maxima, and the M_R/M_s polar plot does not exhibit the well-defined symmetrical lobes encountered for Py^{Si}. These H_c maxima indicate the presence of a cubic anisotropy component. In fact, we have demonstrated in previous studies that a predominant cubic magnetic anisotropy was present in a 10-nm $Fe_{81}Ga_{19}$ film grown on an amorphous glass substrate. It was also shown in that previous study that this cubic character resulted from a (110) crystallographic texture and that it resulted in four maxima in the H_c polar plot [40,48]. Two of the four H_c maxima are along $\varphi = 0°$ and $\varphi = 180°$, showing that one of the cubic easy axes is aligned with H_{dep}. Thus, the angle-dependent study confirms the cubic (i.e., fourfold) anisotropy of $FeGa^{Si}$. It may be noted that, for an $Fe_{81}Ga_{19}$ 20-nm thin film on a GaAs substrate, which exhibited a predominant cubic anisotropy, an H_c value of 25 Oe was previously reported along the easy axis [49].

C. Py/$Fe_{81}Ga_{19}$ on Si

For $Bilayer^{Si}$, the MRev loop shapes along $\varphi = 0°$ and $\varphi = 90°$ exhibit the same characteristics as those for Py, as shown in Fig. 4(a). Indeed, the shape is rectangular

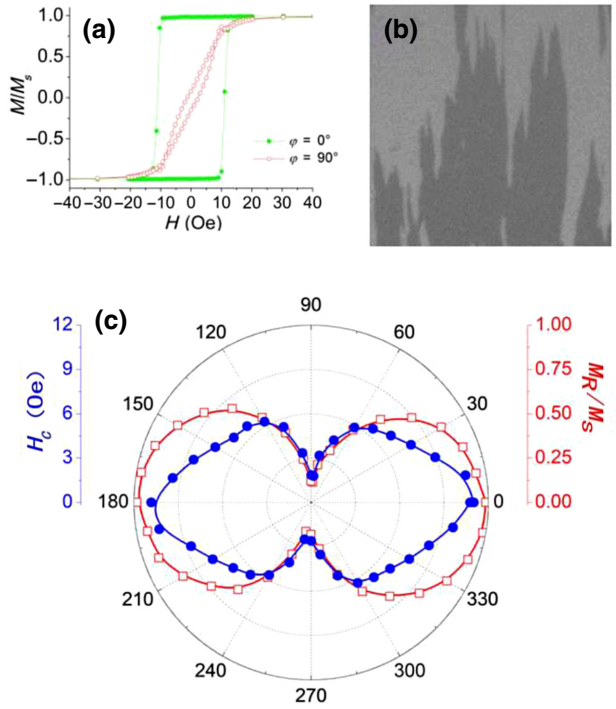

FIG. 4. For Bilayer^{Si}, (a) hysteresis loops measured along $\varphi = 0^\circ$ (filled green circles) and along $\varphi = 90^\circ$ (open red circles); (b) 5 mm × 5 mm MOKE image obtained in the vicinity of the coercive field along $\varphi = 0^\circ$; (c) angular dependence of H_c (filled blue circles) and M_R/M_s (red squares).

along $\varphi = 0^\circ$, and the shape along $\varphi = 90^\circ$ exhibits weak values of H_c and M_R/M_s. These results indicate that the hybrid Bilayer^{Si} system shows a uniaxial character in its anisotropy, driven by the Py layer. An H_c value of 11 Oe is found along $\varphi = 0^\circ$: it is between the value for Py^{Si} (2.8 Oe) and the value for FeGa^{Si} (18 Oe) obtained at the same angle.

The domain pattern for Bilayer^{Si} along $\varphi = 0^\circ$ and in the vicinity of H_c is similar to that for Py^{Si}, as shown in Fig. 4(b). Indeed, it exhibits large domains and zigzag domain walls. The angular dependences of H_c and M_R/M_s are also probed for the bilayer, as shown in Fig. 4(c). The angle-dependent butterfly shape for H_c and the well-defined symmetrical lobes for M_R/M_s confirm the uniaxial anisotropy. The easy axis is along $\varphi = 0^\circ$ and is aligned with H_{dep}. The hybrid system is uniaxial but presents a greater anisotropy constant than does Py^{Si}. It may be noted here that an H_c value of 15 Oe was previously reported for an $Fe_{81}Ga_{19}$(100 nm)/Py(2.5 nm) bilayer grown on Si [35]. This value is in close agreement with the H_c value reported in the present study.

D. Summary of the results for the layers grown on Si substrates

A brief summary is given in this paragraph for the layers grown on Si substrates. Py^{Si} exhibits a uniaxial anisotropy with an EA aligned by and with H_{dep}, and a coercive field of 2.8 Oe along its EA. The domain structure in Py^{Si} corresponds to large domains separated by zigzag domain walls. However, FeGa^{Si} exhibits a cubic anisotropy, with one of the EAs aligned with H_{dep}, and a coercivity value of 18 Oe along this EA. The domain structure in FeGa^{Si} is very different from that in Py^{Si} and exhibits sharp domain walls. Finally, the magnetization reversal in Bilayer^{Si} is similar to that in Py^{Si} in the sense of a similar domain structure and a uniaxial character with an EA (aligned with H_{dep}). The difference between Bilayer^{Si} and Py^{Si} is that there is a greater anisotropy constant for the bilayer: Bilayer^{Si} exhibits a coercivity of 11 Oe along the EA. Still, this coercivity is half of that found in FeGa^{Si} along the same direction. Consequently, the coupling between Py and $Fe_{81}Ga_{19}$ allows a reduction of the coercivity relative to the single $Fe_{81}Ga_{19}$ film, and a drastic change in the character of the anisotropy of the $Fe_{81}Ga_{19}$ layer, as it is uniaxial in the bilayer system. These characteristics render the hybrid bilayer system promising for applications that need to combine a magnetostrictive layer, a uniaxial character, and relatively soft magnetic properties.

TABLE II. Samples on Al substrates studied in Sec. IV. R is the radius of curvature.

Sample name	R	Layer structure
$Py^{R=\infty}$	∞	$Ni_{80}Fe_{20}$(10 nm)/Al
$Py^{R=58\ cm}$	58 cm	$Ni_{80}Fe_{20}$(10 nm)/Al
$Py^{R=24\ cm}$	24 cm	$Ni_{80}Fe_{20}$(10 nm)/Al
$FeGa^{R=\infty}$	∞	$Fe_{81}Ga_{19}$(10 nm)/Al
$FeGa^{R=58\ cm}$	58 cm	$Fe_{81}Ga_{19}$(10 nm)/Al
$FeGa^{R=24\ cm}$	24 cm	$Fe_{81}Ga_{19}$(10 nm)/Al
$Bilayer^{R=\infty}$	∞	$Fe_{81}Ga_{19}$(10 nm)/$Ni_{80}Fe_{20}$(10 nm)/Al
$Bilayer^{R=58\ cm}$	58 cm	$Fe_{81}Ga_{19}$(10 nm)/$Ni_{80}Fe_{20}$(10 nm)/Al
$Bilayer^{R=24\ cm}$	24 cm	$Fe_{81}Ga_{19}$(10 nm)/$Ni_{80}Fe_{20}$(10 nm)/Al

IV. MAGNETIZATION REVERSALS ON FLEXIBLE Al FOILS UNDER MMS

In this section, MRevs of Py, $Fe_{81}Ga_{19}$, and Py/$Fe_{81}Ga_{19}$ layers grown on flexible Al foils are reported. In the following, $\varphi = 0$ when the applied field during the MOKE measurements is in the same direction as H_{dep}, the applied magnetic field during growth. It should be noted here that H_{dep} is applied constantly along the grooves of the Al foils during the growth of the thin films. MMS is applied by sticking the Al foils to convex optical lenses. Each sample is described in Table II. Domain imaging using MOKE can not be performed on Al foils, which may be attributed to the large surface roughness of the Al foils [50]. It should be noted that before measurement, MRev loops are measured on different surface regions to ensure that the Al foils are uniformly bent.

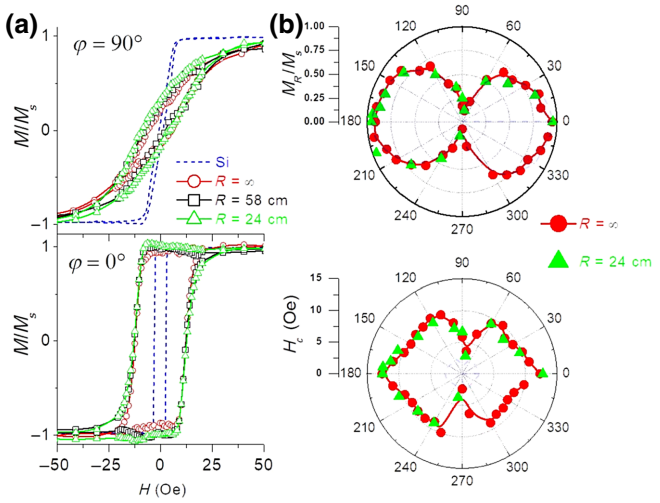

FIG. 5. (a) Hysteresis loops measured along $\varphi = 0°$ (bottom) and along $\varphi = 90°$ (top) for $R = \infty$ (open red circles), $R = 58$ cm (black squares), and $R = 24$ cm (open green triangles) for Py/Al samples. (b) Angular dependence of H_c (bottom) and M_R/M_s (top) for Py on Al foils, for $R = \infty$ (filled red circles) and $R = 24$ cm (filled green triangles).

A. Py on Al

Figure 5(a) shows that the Py MRev loops along $\varphi = 0°$ and $\varphi = 90°$ depend on the nature of the substrate. The coercive and saturation fields have larger values for Al foils than for Py^{Si}. The increase in both fields indicates an increase in the anisotropy constant on Al foils. The shapes of the MRev loops are similar for both substrates, with the presence of a rectangular shape along $\varphi = 0°$. This indicates that the Py layer still exhibits a uniaxial character on flexible Al foils. The MRev loops do not evolve during the application of an isotropic external stress using the two different lenses. This shows the absence of magnetostrictive effects along these two directions at least. It may be noted that the remanence and the coercive field are different from 0 along $\varphi = 90°$. This indicates the presence of an anisotropy dispersion.

The angular dependences of H_c and M_R/M_s are obtained for $Py^{R=24\ cm}$ and $Py^{R=\infty}$, as shown in Fig. 5(b). These angular dependences show an absence of magnetostrictive effects within the plane. Indeed, the H_c and M_R/M_s values with and without MMS are in agreement. The uniaxial anisotropy of Py grown on Al foils is also revealed, as the angular dependence of H_c exhibits a butterflylike shape and the M_R/M_s plot exhibits clear symmetrical lobes. Thus, the Py layers grown on flexible Al are uniaxial and nonmagnetostrictive magnetic thin films, with a greater uniaxial anisotropy constant than for Py^{Si}. This enhancement is likely to arise from the grooved surface morphology of the Al, which would generate a phenomenological shape anisotropy hindering reversal.

B. $Fe_{81}Ga_{19}$ on Al

In a similar manner to the Py MRev loops, the $Fe_{81}Ga_{19}$ MRev loops depend on the nature of the substrate, as shown in Fig. 6(a). The coercive and saturation fields are larger for the Al foil than for the Si substrate. It is noted that previous studies have reported H_c values between 20 and 100 Oe for 50-nm $Fe_{81}Ga_{19}$ films grown on flexible polyethylene terephthalate substrates, depending on the growth conditions [11–19]. However, there are major differences between the MRevs of the Py samples on Al foils and the $Fe_{81}Ga_{19}$ ones. Indeed, the MRevs of $Fe_{81}Ga_{19}$ are modified when MMS is applied. The MRev loop shapes, coercivities, and saturation fields are very different for $R = \infty$, $R = 24$ cm, and $R = 58$ cm. This shows that magnetostrictive effects are important for $Fe_{81}Ga_{19}$ thin films. This is expected from the magnetostrictive properties of $Fe_{81}Ga_{19}$. In a previous publication [48], the magnetostrictive stress $|b_{eff}|$ and the magnetostrictive strain λ_{eff} for a 10-nm $Fe_{81}Ga_{19}$ thin film were reported. At saturation, $|b_{eff}|$ (λ_{eff}) was found to be 1.2 MPa (16 ppm). These values are close to those previously reported ($\lambda_{eff} \sim 20$ ppm for similar layer thicknesses) [2,51–53]. Also, some other reported values for $|b_{eff}|$ (and/or λ_{eff}) in $Fe_{81}Ga_{19}$ epitaxial thin films were found to be larger [54,55]. In these studies, the larger values were attributed to crystallographic properties driven by the epitaxy. In the present study, it should be noted that the observed effects of MMS on the $Fe_{81}Ga_{19}$ MRev loops are irreversible: the MRev properties remain constant after the bending has been performed. The sample, after bending and being flattened back again, does not exhibit the initial MRev properties (i.e., those of $FeGa^{R=\infty}$) but retains the properties observed when curved on the lenses.

To further understand the evolution of the anisotropic properties with the nature of the substrate and with MMS, the angular dependences of H_c and M_R/M_s are probed and are presented in Fig. 6(b). The angular dependence of H_c for $FeGa^{R=\infty}$ exhibits four maxima, revealing that the cubic character of the anisotropy observed in $FeGa^{Si}$ is still present. However, the shape of the angular dependence of H_c for $FeGa^{R=\infty}$ is elongated along φ=0° relative to that for $FeGa^{Si}$.

To understand this elongation phenomenon, simulations are performed using a modified Stoner and Wohlfarth (SW) model [56,57], implemented in a software package named StoneX [46,47,58]. This model can be considered as a modification of the coherent rotational SW model of MRevs, as it includes a random anisotropy, which was not considered in the initial SW model [56,57]. The ferromagnetic material has a magnetic moment per unit volume $M_F\vec{e}_F$, which makes an angle θ with the twofold anisotropy axis [46,47,58]. A value of M_F of 920 kA/m is determined by measurements with a VSM and a superconducting quantum interference device on these samples. The F domain possesses a twofold anisotropy axis along

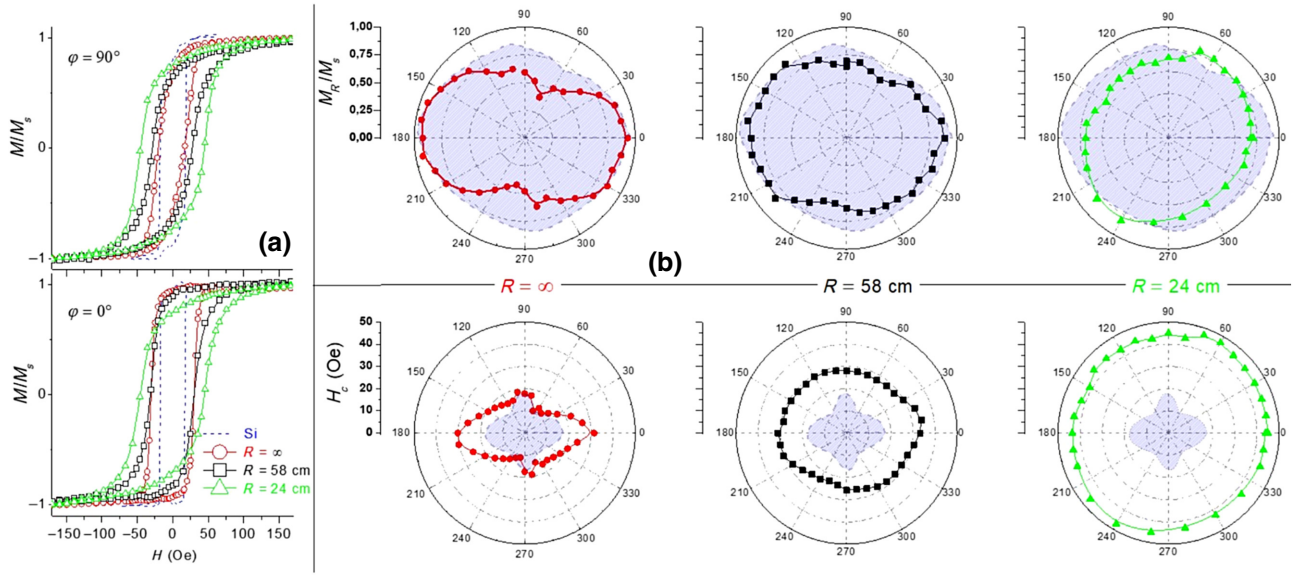

FIG. 6. (a) Hysteresis loops measured along $\varphi = 0°$ (bottom) and along $\varphi = 90°$ (top) for $Fe_{81}Ga_{19}$/Al samples with $R = \infty$ (open red circles), $R = 58$ cm (black squares), and $R = 24$ cm (green triangles), and also for the $Fe_{81}Ga_{19}$/Si sample (blue dashed line). (b) Angular dependence of H_c (bottom row) and M_R/M_s (top row) for $Fe_{81}Ga_{19}$ on Al foils, for $R = \infty$ (left column), $R = 58$ cm (middle column), and $R = 24$ cm (right column). The shaded areas are a guide to the eye to show the physical quantities (i.e., H_c or M_R/M_s) obtained from $FeGa^{Si}$.

$\vec{e}_{ua}$, which defines the uniaxial EA. The F domain also possesses fourfold (i.e., cubic) anisotropy axes. Finally, it possesses a random anisotropy, to allow one to consider the presence of a randomly distributed anisotropy axis [59–61] or a rotatable anisotropy axis [62–64]. The EA is located at an angle φ relative to the external field $H\vec{e}_x$. The EA is parallel to one of the cubic easy axes. The total free energy $\mathcal{F}$ per unit volume considered in the model is then given by adding the Zeeman and anisotropy energy densities:

$$\mathcal{F}(\theta) = -\mu_0 H M_F \cos(\theta + \varphi) + K_2 \sin^2(\theta) + K_4 \sin^2(\theta)\cos^2(\theta) + K_r \sin^2(\theta + \varphi). \quad (1)$$

Here, K_2 is the uniaxial anisotropy constant, K_4 is the cubic anisotropy constant, and K_r is the random anisotropy constant. Using the parameters presented in Table III, this model reproduces the angular dependence of H_c, including the elongation phenomenon, as shown in Fig. 7. The difference between the parameters for $FeGa^{R=\infty}$ and $FeGa^{Si}$ lies in an enhancement of the value of the random anisotropy constant and the appearance of a uniaxial constant for $FeGa^{R=\infty}$. The $FeGa^{Si}$ thin film is a polycrystalline thin film with a (110) preferential orientation [48]. The (110) preferential orientation provides a cubic character to the anisotropy. However, as this orientation is only preferential, it has a random character related to the polycrystalline nature. This crystallographic texture, related to the phenomenon of anisotropy in $Fe_{81}Ga_{19}$ thin films, was shown and discussed in greater detail in Ref. [48]. Our theoretical model provides a quantification of the anisotropy constant related to this phenomenon. A random character in the anisotropy cannot induce an elongation, due to symmetry considerations (as it is not angle dependent). Thus, the elongation phenomenon is driven by the development of a uniaxial anisotropy in the samples on Al foils. Also, the angular dependence of M_R/M_s for $FeGa^{R=\infty}$ is elongated along $\varphi = 0°$ relative to that for $FeGa^{Si}$. This confirms the development of a uniaxial character for $FeGa^{R=\infty}$. These modifications of the character of the anisotropy for the $Fe_{81}Ga_{19}$ layer, such as an enhancement of the uniaxial constant of Py observed on the same surface, support a uniaxial mechanism driven by the substrate morphology, i.e., the grooved morphology of the Al foils. Furthermore, a previous study of $Fe_{81}Ga_{19}$ thin films grown on a wrinkled surface also identified surface morphology as a driving mechanism for the anisotropic properties [65]. Our study shows that Al foils with grooved surfaces may be used to develop a uniaxial character in an $Fe_{81}Ga_{19}$ thin film.

It should be noted that the anisotropy-constant calculations presented here are performed with a model assuming a coherent rotational MRev. Such a coherent rotational model is an appropriate approximation when the activation

TABLE III. Physical parameters used in the simulations.

	$M_F = 920$ kA m^{-1}		
	K_2 (kJ m^{-3})	K_4 (kJ m^{-3})	K_r (kJ m^{-3})
$FeGa^{Si}$	0.000	0.246	0.608
$FeGa^{R=\infty}$	0.280	0.246	0.950

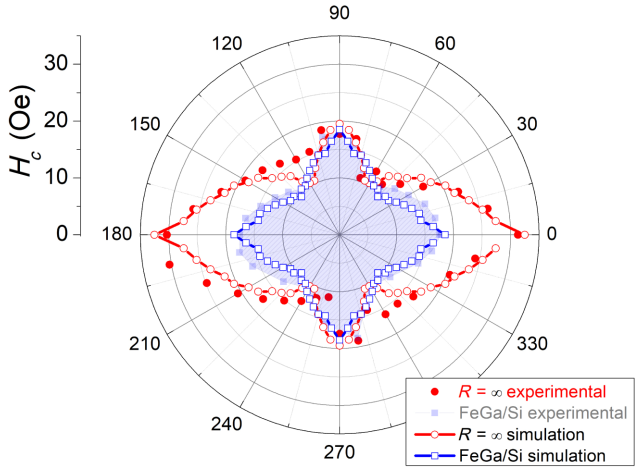

FIG. 7. Experimental (filled red circles) and simulated (open red circles) angular dependences of H_c for $FeGa^{R=\infty}$, and experimental (filled gray squares) and simulated (blue squares) angular dependences of H_c for $FeGa^{Si}$. The shaded area is a guide to the eye to indicate the H_c obtained from $FeGa^{Si}$.

fields of domain walls do not differ strongly from the critical fields estimated by the macrospin model. In Py thin films, it is often observed that the coherent rotational model does not hold, as it overestimates activation fields at and around the easy axis. In our study, we find that a coherent approximation involving uniaxial, cubic, and random anisotopies is not sufficient to describe the angle-dependent MRevs when the samples contain a Py layer.

When MMS is applied and increased in magnitude, the elongations observed in the angular dependence of H_c and M_R/M_s vanish. In particular, the shape of the angular dependence of H_c becomes increasingly more circular, as shown in Fig. 6(b). The combined circular shapes of M_R/M_s and H_c are characteristics of a random distribution of anisotropy axes. Here, these phenomena are observed and indicate that the character of the anisotropy becomes randomized by the MMS. This is confirmed by very similar loops observed along 0° and 90° for $FeGa^{R=24\ cm}$, as shown in Fig. 6(a). It should also be noted that the H_c values increase when MMS is applied, indicating an increase in the magnitude of the anisotropy constant. These observed effects of MMS on the angular dependences are irreversible: the properties of the angular dependences remain constant after the bending has been performed. The sample, after bending and being flattened back again, does not exhibit the initial MRev properties (i.e., those of $FeGa^{R=\infty}$) but retains the properties observed when on the lenses.

To summarize the $Fe_{81}Ga_{19}$ results, the 10-nm thin film grown on Si exhibits a cubic anisotropy, which is maintained when it is grown on a flat Al foil. The coercivity observed for $Fe_{81}Ga_{19}$ grown on Si is remarkably increased in the direction parallel to the Al grooves. This indicates a uniaxial anisotropy induced by the striped surface morphology of the Al. A MMS applied to the flexible system results in a progressive increase in the random character of the anisotropy towards complete randomization for the greatest curvature. Also, MMS results in coercivity enhancements. All of these MMS effects are irreversible, which allows long-lasting MRev properties.

C. Py/$Fe_{81}Ga_{19}$ on Al

In a similar manner to the Py and $Fe_{81}Ga_{19}$ thin films, the MRevs in Py/$Fe_{81}Ga_{19}$ along and perpendicular to H_{dep} depend on the nature of the substrate. The coercive and saturation fields are larger for the Al foil than for the Si substrate, as shown in Fig. 8(a). The MRevs are modified when MMS is applied. Indeed, the MRev loop shapes, coercivities, and saturation fields are very different between $Bilayer^{R=\infty}$, $Bilayer^{R=58\ cm}$, and $Bilayer^{R=24\ cm}$. This indicates that magnetostrictive effects are important for the bilayers. These observed effects of MMS on the angular dependences for the bilayer are irreversible.

To further understand these phenomena, the angular dependences of H_c and M_R/M_s are probed and are shown in Fig. 8(b). The angular dependence of H_c exhibits a butterfly shape, and M_R/M_s exhibits well-defined symmetrical lobes when no MMS is applied (i.e., for $R = \infty$). These characteristics show that the MRev in $Bilayer^{R=\infty}$ is driven by a uniaxial character, as observed for $Bilayer^{Si}$. An enhancement of the uniaxial anisotropy constant of the bilayer is observed when the bilayer is grown on an Al foil, as shown by greater H_c values for $Bilayer^{R=\infty}$ than for $Bilayer^{Si}$. When MMS is applied and increased in magnitude, the angular dependence of H_c evolves from a butterflylike shape to an ellipsoidlike shape. This indicates the development of a random anisotropy. This random-anisotropy effect under MMS is confirmed by the evolution of the angular dependence of M_R/M_s, which exhibits a loss of the two-lobe geometry upon MMS. It should be noted that the coercivity enhancement due to MMS is strongly angle dependent here and shows a minimum along the Al stripes. Also, angle-dependent circular shapes are not observed, whereas they are present in the $Fe_{81}Ga_{19}$ case. The observed randomization due to MMS, i.e., the inverse magnetostrictive effect, is not as effective for the bilayer as it is for a single $Fe_{81}Ga_{19}$ film. These observed effects of MMS on the angular dependences for the bilayer are irreversible.

To summarize the results for the hybrid system, the 10-nm thin film grown on Si exhibits a uniaxial anisotropy, which is maintained when it is grown on the Al foil. In a similar manner to the single $Fe_{81}Ga_{19}$ layer and the single Py layer, the coercive fields observed on Si are increased when the $Fe_{81}Ga_{19}$ is grown on flexible Al. When MMS is applied, the hybrid system shows neither the random anisotropy dispersion observed for $Fe_{81}Ga_{19}$

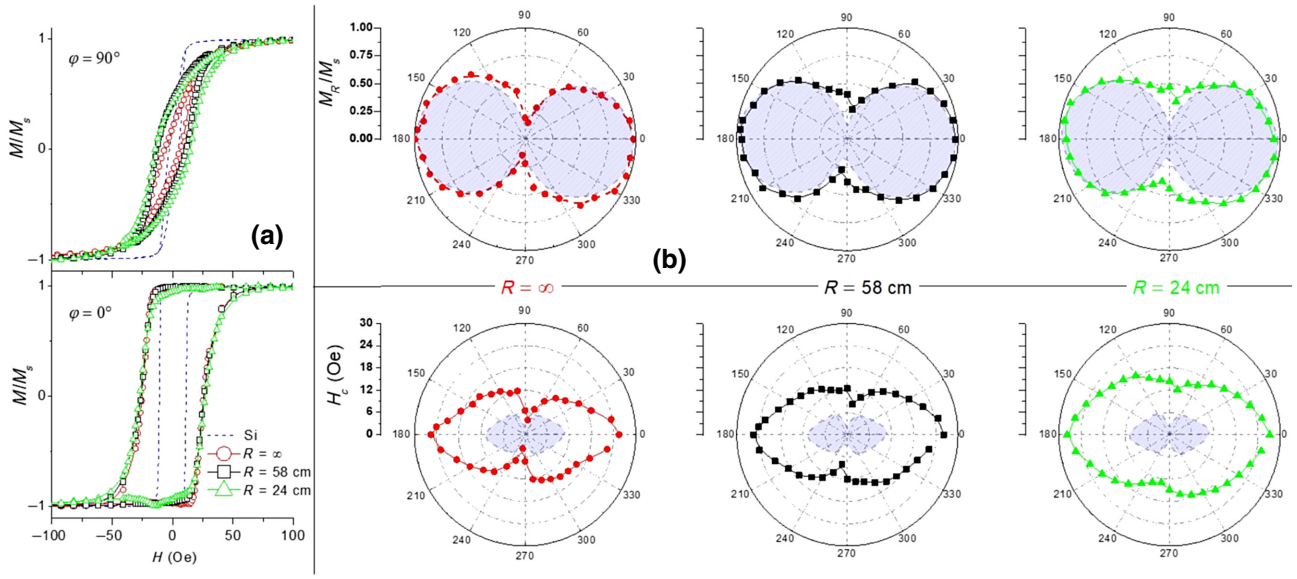

FIG. 8. (a) Hysteresis loops measured along $\varphi = 0°$ (bottom) and along $\varphi = 90°$ (top) for $Fe_{81}Ga_{19}$/Py/Al samples with $R = \infty$ (open red circles), $R = 58$ cm (black squares), and $R = 24$ cm (green triangles), and also for the $Fe_{81}Ga_{19}$/Py/Si sample (blue dashed line). (b) Angular dependence of H_c (bottom row) and M_R/M_s (top row) for $Fe_{81}Ga_{19}$ on Al foils, for $R = \infty$ (left column, filled red circles), $R = 58$ cm (middle column, filled black squares), and $R = 24$ cm (right column, filled green triangles). The shaded areas are a guide to the eye to indicate the physical quantities (i.e., H_c or M_R/M_s) obtained from Bilayer^{Si}.

thin films nor the MMS-independent uniaxial character observed for the nonmagnetostrictive Py, but exhibits a magnetostrictive effect that is strongly angle dependent. The absence of cracks or other structural defects due to the bending and the observed MMS effects presented in this paper should be considered together with the irreversible UMS effects previously reported. These points highlight the key role of permanent plastic residual strain in modifying the magnetization-reversal properties of $Fe_{81}Ga_{19}$. This is further supported by the unmodified MRevs in the nonmagnetostrictive Py single layer in the presence of bending. Since all these MMS effects are irreversible, this allows long-lasting tailoring of the MRev properties of the bilayer.

V. CONCLUSION

In the study presented in this paper, a 10-nm $Fe_{81}Ga_{19}$ thin film, a 10-nm Py thin film, and an $Fe_{81}Ga_{19}$(10 nm)/Py(10 nm) bilayer are grown on Si substrates and on flexible Al foils. Samples grown on flexible Al foils are subjected to MMS through the use of convex optical lenses.

The Py^{Si} sample exhibits a uniaxial anisotropy, with the EA aligned with H_{dep}. Its domain structure around H_c corresponds to large domains separated by sawtooth domain walls. FeGa^{Si} exhibits a cubic anisotropy, with one of the EAs aligned with H_{dep}. Its domain structure around H_c exhibits sharp domain walls with a right-angle geometry. The magnetization reversal in Bilayer^{Si} is similar to that in Py^{Si} in the sense of a similar domain structure and a uniaxial character, with an EA aligned by and with H_{dep}. Bilayer^{Si} exhibits a greater anisotropy constant than Py^{Si}, and has a reduced coercivity compared with the single $Fe_{81}Ga_{19}$ layer on Si. The coupling between Py and $Fe_{81}Ga_{19}$ allows a reduced coercivity and a drastic change in the character of the anisotropy. These characteristics render the hybrid bilayer system promising for applications that need to combine magnetostriction with relatively soft uniaxial magnetic properties.

For all of the layered structures, it is found that the MRevs depend on the nature of the substrate. All layers grown on Al foils show a development or enhancement of the uniaxial character. This effect originates from the surface morphology, with an EA lying along the Al grooves. MMS applied to flexible samples on Al foils results in very different effects as a function of the composition of the layered system. For Py, MMS has no effect, as expected for a nonmagnetostrictive system. For $Fe_{81}Ga_{19}$, MMS results in a full in-plane randomization of the MRev properties. It increases the anisotropy of the system. For the bilayer, the MMS applied results in a randomization of the anisotropy. However, MMS does not fully randomize the MRev properties, and the bilayer retains a uniaxial character. MMS also results in an increase in the anisotropy. The use of MMS to modify the anisotropic character of $Fe_{81}Ga_{19}$-based systems is demonstrated here. A wide range of effects can be obtained as a function of the nature of the system and as a function of the MMS strength. All these

effects are irreversible. These MMS effects can be used to tailor and modify the MRev properties of $Fe_{81}Ga_{19}$-based systems in a permanent manner.

The drawback of using Al foils is their metallic nature, which renders some applications difficult, if not impossible, to realize. For instance, the magnetoresistance of nanometric layered systems based on $Fe_{81}Ga_{19}$ would be extremely difficult to detect once the system was deposited on a thick metallic layer. To go beyond the findings of our study, further work involving MMS effects with either an insulator as a buffer layer or an insulating flexible substrate could be of interest.

ACKNOWLEDGMENTS

The authors thank Q. Spenato for the schematic illustration in Fig. 1(b), which was realized using Blender. The authors thank P. Elies, at the Université de Bretagne Occidentale, and B. Warot Fontrose and R. Cours, at the Centre d'Elaboration de Materiaux et d'Etudes Structurales, for microscopy measurements and analysis. The program used for the simulation presented in this paper is open-source software written in Python [66], using the Scipy [67] and Matplotlib [68] libraries. The source code is freely available under the GPLv3 license [69]. A.R.E.P. and C.J.S. want to thank the RSA NRF (Grants No. 120856 and No. 80880) and UJ for funding support.

[1] Chaitanya Mudivarthi, Supratik Datta, Jayasimha Atulasimha, Phillip G. Evans, Marcelo J. Dapino, and Alison B. Flatau, Anisotropy of constrained magnetostrictive materials, J. Magn. Magn. Mater. **322**, 3028 (2010).

[2] S. U. Jen and C. C. Liu, Magneto-elastic and magnetic domain properties of $Fe_{81}Ga_{19}$/Si(100) films, J. Appl. Phys. **115**, 013909 (2014).

[3] Arthur E. Clark, James B. Restorff, Marilyn Wun-Fogle, Thomas A. Lograsso, and Deborah L. Schlagel, Magnetostrictive properties of body-centered cubic Fe-Ga and Fe-Ga-Al alloys, IEEE Trans. Magn. **36**, 3238 (2000).

[4] Jayasimha Atulasimha and Alison B Flatau, A review of magnetostrictive iron–gallium alloys, Smart Mater. Struct. **20**, 043001 (2011).

[5] Fumio Narita and Marina Fox, A review on piezoelectric, magnetostrictive, and magnetoelectric materials and device technologies for energy harvesting applications, Adv. Eng. Mater. **20**, 1700743 (2018).

[6] Ping Sheng, Baomin Wang, and Runwei Li, Flexible magnetic thin films and devices, J. Semicond. **39**, 011006 (2018).

[7] Liu Yi-Wei, Zhan Qing-Feng, and Li Run-Wei, Fabrication, properties, and applications of flexible magnetic films, Chin. Phys. B **22**, 127502 (2013).

[8] Y. Zheng, X. Ding, C. C. Y. Poon, B. P. L. Lo, H. Zhang, X. Zhou, G. Yang, N. Zhao, and Y. Zhang, Unobtrusive sensing and wearable devices for health informatics, IEEE Trans. Biomed. Eng. **61**, 1538 (2014).

[9] Michael Melzer, Jens Ingolf Mönch, Denys Makarov, Yevhen Zabila, Gilbert Santiago Cañó Bermúdez, Daniil Karnaushenko, Stefan Baunack, Falk Bahr, Chenglin Yan, Martin Kaltenbrunner, and Oliver G. Schmidt, Wearable magnetic field sensors for flexible electronics, Adv. Mater. **27**, 1274 (2015).

[10] Noel D'Souza, Ayan Biswas, Hasnain Ahmad, Mohammad Salehi Fashami, Md Mamun Al-Rashid, Vimal Sampath, Dhritiman Bhattacharya, Md Ahsanul Abeed, Jayasimha Atulasimha, and Supriyo Bandyopadhyay, Energy-efficient switching of nanomagnets for computing: Straintronics and other methodologies, Nanotechnology **29**, 442001 (2018).

[11] Guohong Dai, Qingfeng Zhan, Yiwei Liu, Huali Yang, Xiaoshan Zhang, Bin Chen, and Run-Wei Li, Mechanically tunable magnetic properties of $Fe_{81}Ga_{19}$ films grown on flexible substrates, Appl. Phys. Lett. **100**, 122407 (2012).

[12] Xiaoshan Zhang, Qingfeng Zhan, Guohong Dai, Yiwei Liu, Zhenghu Zuo, Huali Yang, Bin Chen, and Run-Wei Li, Effect of buffer layer and external stress on magnetic properties of flexible FeGa films, J. Appl. Phys. **113**, 17A901 (2013).

[13] Guohong Dai, Qingfeng Zhan, Huali Yang, Yiwei Liu, Xiaoshan Zhang, Zhenghu Zuo, Bin Chen, and Run-Wei Li, Controllable strain-induced uniaxial anisotropy of $Fe_{81}Ga_{19}$ films deposited on flexible bowed-substrates, J. Appl. Phys. **114**, 173913 (2013).

[14] Ying Yu, Qingfeng Zhan, Jinwu Wei, Jianbo Wang, Guohong Dai, Zhenghu Zuo, Xiaoshan Zhang, Yiwei Liu, Huali Yang, Yao Zhang, Shuhong Xie, Baomin Wang, and Run-Wei Li, Static and high frequency magnetic properties of FeGa thin films deposited on convex flexible substrates, Appl. Phys. Lett. **106**, 162405 (2015).

[15] Derang Cao, Zhenkun Wang, Lining Pan, Hongmei Feng, Xiaohong Cheng, Zengtai Zhu, Jianbo Wang, Qingfang Liu, and Genliang Han, Controllable magnetic and magnetostrictive properties of FeGa films electrodeposited on curvature substrates, Appl. Phys. A **122**, 938 (2016).

[16] Yi Zhang, Chaojuan Huang, Mutellip Turghun, Zhihua Duan, Feifei Wang, and Wangzhou Shi, Electric-regulated enhanced in-plane uniaxial anisotropy in FeGa/PMN-PT composite using oblique pulsed laser deposition, Appl. Phys. A **124**, 289 (2018).

[17] Guohong Dai, Xiangjun Xing, Yun Shen, and Xiaohua Deng, Stress tunable magnetic stripe domains in flexible $Fe_{81}Ga_{19}$ films, J. Phys. D: Appl. Phys. **53**, 055001 (2019).

[18] D. P. Pattnaik, R. P. Beardsley, C. Love, S. A. Cavill, K. W. Edmonds, and A. W. Rushforth, Multilevel information storage using magnetoelastic layer stacks, Sci. Rep. **9**, 3156 (2019).

[19] I. Hontecillas, I. Figueruelo, S. Abad, and R. Ranchal, Tuning the magnetic anisotropy of Ga-rich FeGa thin films deposited on rigid substrates, J. Magn. Magn. Mater. **494**, 165771 (2020).

[20] A. Layadi, Effect of multiaxial stress in thin films on the ferromagnetic resonance mode characteristics, J. Appl. Phys. **127**, 223907 (2020).

[21] P. Rasilo, U. Aydin, F. Martin, A. Belahcen, R. Kouhia, and L. Daniel, Equivalent strain and stress models for the effect of mechanical loading on the permeability of ferromagnetic materials, IEEE Trans. Magn. **55**, 1 (2019).

[22] Laurent Daniel, An analytical model for the magnetostriction strain of ferromagnetic materials subjected to multiaxial stress, Eur. Phys. J. Appl. Phys. **83**, 30904 (2018).
[23] Artjom Avakian and Andreas Ricoeur, An extended constitutive model for nonlinear reversible ferromagnetic behaviour under magnetomechanical multiaxial loading conditions, J. Appl. Phys. **121**, 053901 (2017).
[24] Y. Chang, C. Hsu, H. Chu, and C. Tseng, Magnetomechanical vibrations of three-phase three-leg transformer with different amorphous-cored structures, IEEE Trans. Magn. **47**, 2780 (2011).
[25] B. Rezaeealam, T. Ueno, and S. Yamada, Quasi-static finite element analysis of magnetostrictive vibration energy harvester, J. Magn. Soc. Jpn. **36**, 155 (2012).
[26] Haomin Chen, Ying Jing, Jeng-Hun Lee, Dan Liu, Jungmo Kim, Shusheng Chen, Kan Huang, Xi Shen, Qingbin Zheng, Jinglei Yang, Seokwoo Jeon, and Jang-Kyo Kim, Human skin-inspired integrated multidimensional sensors based on highly anisotropic structures, Mater. Horiz. **7**, 2378 (2020).
[27] Kyuyoung Kim, Junseong Ahn, Yongrok Jeong, Jungrak Choi, Osman Gul, and Inkyu Park, All-soft multiaxial force sensor based on liquid metal for electronic skin, Micro and Nano Syst. Lett. **9**, 2 (2021).
[28] Hongbian Li, Suye Lv, and Ying Fang, Bio-inspired micro/nanostructures for flexible and stretchable electronics, Nano Res. **13**, 1244 (2020).
[29] Kahyun Sun, Hangil Ko, Hyun-Ha Park, Minho Seong, Sang-Hyeon Lee, Hoon Yi Hyung Wook Park, Tae-il Kim, Changhyun Pang, and Hoon Eui Jeong, Hybrid architectures of heterogeneous carbon nanotube composite microstructures enable multiaxial strain perception with high sensitivity and ultrabroad sensing range, Small **14**, 1803411 (2018).
[30] H. R Le and M. P. F Sutcliffe, Analysis of surface roughness of cold-rolled aluminium foil, Wear **244**, 71 (2000).
[31] R. Ranchal and V. González-Martín, Investigation on the structural and magnetic properties of sputtered $TbFe_2/Fe_3Ga$ heterostructures, J. Appl. Phys. **110**, 053901 (2011).
[32] R. Ranchal, V. Gutiérrez-Díez, and V. González Martín, Influence of the $TbFe_2$ crystallization on the magnetic and magnetostrictive properties of $(Fe_3Ga/TbFe_2)n$ heterostructures, Acta Mater. **60**, 1840 (2012).
[33] N. Lupu, H. Chiriac, and P. Pascariu, Electrochemical deposition of FeGA/NiFe magnetic multilayered films and nanowire arrays, J. Appl. Phys. **103**, 07B511 (2008).
[34] Colin R. Rementer, Kevin Fitzell, Qiang Xu, Paul Nordeen, Gregory P. Carman, Yuanxun E. Wang, and Jane P. Chang, Tuning static and dynamic properties of FeGa/NiFe heterostructures, Appl. Phys. Lett. **110**, 242403 (2017).
[35] Adrian Acosta, Kevin Fitzell, Joseph D. Schneider, Cunzheng Dong, Zhi Yao, Ryan Sheil, Yuanxun Ethan Wang, Gregory P. Carman, Nian X. Sun, and Jane P. Chang, Underlayer effect on the soft magnetic, high frequency, and magnetostrictive properties of FeGa thin films, J. Appl. Phys. **128**, 013903 (2020).
[36] BTelectronics: 'Bt electronics, ' https://bt-electronics.com/ (2020).
[37] Luca Callegaro, Ezio Puppin, and Davide Petrali, A cell for in-plane, isotropic external stressing of thin films: Inverse magnetoelastic effects, Rev. Sci. Instrum. **68**, 1796 (1997).
[38] Luca Callegaro and Ezio Puppin, Isotropic strain and magnetic properties in ni films, Phys. Rev. B **59**, 146 (1999).
[39] EvicoMagneticsGmbH: 'Evicomagneticsgmbh,' http://evicomagnetics.com/ (2020).
[40] W. Jahjah, J.-Ph. Jay, Y. Le Grand, A. Fessant, A. R. E. Prinsloo, C. J. Sheppard, D. T. Dekadjevi, and D. Spenato, Electrical Manipulation of Magnetic Anisotropy in a $Fe_81Ga_19/Pb(Mg_1/3Nb_2/3)O_3$-$Pb(Zr_xTi_{1-x})O_3$ Magnetoelectric Multiferroic Composite, Phys. Rev. Appl. **13**, 034015 (2020).
[41] J. P. Nibarger, R. Lopusnik, Z. Celinski, and T. J. Silva, Variation of magnetization and the Landé g factor with thickness in Ni–Ge films, Appl. Phys. Lett. **83**, 93 (2003).
[42] C Favieres, J Vergara, and V Madurga, Charged magnetic domain walls as observed in nanostructured thin films: Dependence on both film thickness and anisotropy, J. Phys.: Condens. Matter **25**, 066002 (2013).
[43] Alex Hubert and Rudolf Schäfer, *Magnetic Domains* (Springer, Berlin, Germany, 2009), p. 427.
[44] Y. Lee, A. R. Koymen, and M. J. Haji-Sheikh, Discovery of cross-tie walls at saw-tooth magnetic domain boundaries in permalloy films, Appl. Phys. Lett. **72**, 851 (1998).
[45] Alex Hubert and Rudolf Schäfer, *Magnetic Domains* (Springer, Berlin, Germany, 2009), p. 263.
[46] N. Ryon, J. Richy, C. J. Sheppard, A. R. E. Prinsloo, A. Fessant, J.-Ph. Jay, D. Spenato, and D. T. Dekadjevi, Thermal simulation of magnetization reversals for a size-distributed assembly of nanoparticles with uniaxial and cubic anisotropies, J. Appl. Phys. **126**, 133901 (2019).
[47] J. Richy, J. Ph. Jay, S. P. Pogossian, J. Ben Youssef, C. J. Sheppard, A. R. E. Prinsloo, D. Spenato, and D. T. Dekadjevi, Thermal simulation of magnetization reversals for size-distributed assemblies of core-shell exchange biased nanoparticles, J. Appl. Phys. **120**, 083905 (2016).
[48] W. Jahjah, R. Manach, Y. Le Grand, A. Fessant, B. Warot-Fonrose, A. R. E. Prinsloo, C. J. Sheppard, D. T. Dekadjevi, D. Spenato, and J.-Ph. Jay, Thickness Dependence of Magnetization Reversal and Magnetostriction in Fe_81Ga_19 Thin Films, Phys. Rev. Appl. **12**, 024020 (2019).
[49] D. E. Parkes, S. A. Cavill, A. T. Hindmarch, P. Wadley, F. McGee, C. R. Staddon, K. W. Edmonds, R. P. Campion, B. L. Gallagher, and A. W. Rushforth, Non-volatile voltage control of magnetization and magnetic domain walls in magnetostrictive epitaxial thin films, Appl. Phys. Lett. **101**, 072402 (2012).
[50] Douglas Natelson, *Nanostructures and Nanotechnology* (Cambridge University Press, Cambridge, United Kingdom, 2015), p. 320.
[51] A. Javed, N. A. Morley, and M. R. J. Gibbs, Thickness dependence of magnetic and structural properties in $Fe_{80}Ga_{20}$ thin films, J. Appl. Phys. **107**, 09A944 (2010).
[52] Yasushi Endo, Takumi Sakai, Takamichi Miyazaki, and Yutaka Shimada, Effect of film thickness on the high frequency magnetic properties of polycrystalline Fe–Ga films, IEEE Trans. Magn. **53**, 5 (2017).
[53] Ying Yu, Qingfeng Zhan, Jinwu Wei, Jianbo Wang, Guohong Dai, Zhenghu Zuo, Xiaoshan Zhang, Yiwei Liu, Huali

Yang, Yao Zhang, Shuhong Xie, Baomin Wang, and Run-Wei Li, Static and high frequency magnetic properties of FeGa thin films deposited on convex flexible substrates, Appl. Phys. Lett. **106**, 162405 (2015).

[54] D. E. Parkes, L. R. Shelford, P. Wadley, V. Holý, M. Wang, A. T. Hindmarch, G. van der Laan, R. P. Campion, K. W. Edmonds, S. A. Cavill, and A. W. Rushforth, Magnetostrictive thin films for microwave spintronics, Sci. Rep. **3**, 1 (2013).

[55] M. Barturen, D. Sander, J. Milano, J. Premper, C. Helman, M. Eddrief, J. Kirschner, and M. Marangolo, Bulklike behavior of magnetoelasticity in epitaxial $Fe_{1-x}Ga_x$ thin films, Phys. Rev. B **99**, 134432 (2019).

[56] E. C. Stoner and E. P. Wohlfarth, Interpretation of high coercivity in ferromagnetic materials, Nature **160**, 650 (1947).

[57] E. C. Stoner and E. P. Wohlfarth, A mechanism of magnetic hysteresis in heterogeneous alloys, Philos. Trans. R. Soc., A **240**, 599 (1948).

[58] J. Richy, Stonex, https://github.com/LabMagUBO/StoneX (2016).

[59] R. Alben, J. J. Becker, and M. C. Chi, Random anisotropy in amorphous ferromagnets, J. Appl. Phys. **49**, 1653 (1978).

[60] Giselher Herzer, Anisotropies in soft magnetic nanocrystalline alloys, J. Magn. Magn. Mater. **294**, 99 (2005). nANO2004.

[61] A. Sukhov, K. D. Usadel, and U. Nowak, Ferromagnetic resonance in an ensemble of nanoparticles with randomly distributed anisotropy axes, J. Magn. Magn. Mater. **320**, 31 (2008).

[62] S. Tacchi, S. Fin, G. Carlotti, G. Gubbiotti, M. Madami, M. Barturen, M. Marangolo, M. Eddrief, D. Bisero, A. Rettori, and M. G. Pini, Rotatable magnetic anisotropy in a $Fe_0.8Ga_0.2$ thin film with stripe domains: Dynamics versus statics, Phys. Rev. B **89**, 024411 (2014).

[63] Guozhi Chai, Nguyen N. Phuoc, and C. K. Ong, Exchange coupling driven omnidirectional rotatable anisotropy in ferrite doped CoFe thin film, Sci. Rep. **2**, 832 (2012).

[64] J. Geshev, L. G. Pereira, and J. E. Schmidt, Rotatable anisotropy and coercivity in exchange-bias bilayers, Phys. Rev. B **66**, 134432 (2002).

[65] Shuanglan Zhang, Qingfeng Zhan, Ying Yu, Luping Liu, Huihui Li, Huali Yang, Yali Xie, Baomin Wang, Shuhong Xie, and Run-Wei Li, Surface morphology and magnetic property of wrinkled FeGa thin films fabricated on elastic polydimethylsiloxane, Appl. Phys. Lett. **108**, 102409 (2016).

[66] Travis E. Oliphant, Python for scientific computing, Comput. Sci. Eng. **9**, 10 (2007).

[67] Stefan Van Der Walt, S. Chris Colbert, and Gaël Varoquaux, The NumPy array: A structure for efficient numerical computation, Comput. Sci. Eng. **13**, 2 (2011).

[68] John D. Hunter, Matplotlib: A 2D graphics environment, Comput. Sci. Eng. **9**, 90 (2007).

[69] https://github.com/LabMagUBO/StoneX